In: 2007 IEEE International Conference on Robotics and Automation (ICRA'07) / 10-14 April 2007 / Rome, Italy

Robot-Based 3D Ultrasound Scanning and Registration with Infrared Navigation Support

Philipp J. STOLKA[1], Michel WARINGO[1], Dominik HENRICH[1], Steffen H. TRETBAR[2], and Philipp A. FEDERSPIL[2]

1: Lehrstuhl für Angewandte Informatik III
(Robotik und Eingebettete Systeme)
Universität Bayreuth, D-95447 Bayreuth, Germany
{philipp.stolka, michel.waringo, dominik.henrich}
@uni-bayreuth.de

2: Universitäts-Hals-Nasen-Ohrenklinik Heidelberg
D-69120 Heidelberg, Germany
federspil@med.uni-heidelberg.de
steffen.tretbar@ibmt.fraunhofer.de

Abstract – Surgical procedures with navigation or robot system support usually require pre-operative planning data. This data can be acquired with imaging techniques such as computed tomography (CT), the current gold standard due to its high precision. With such imaging data, access trajectories, implant positions, individual milling paths etc. can be computed. We present a novel ultrasound-based method to generate 3D image data which is well-suited for many interventions, but less costly than equivalent CT data. The method's feasibility is demonstrated for robot-based implant bed milling in the lateral skull base, in a process consisting of infrared navigation registration, manual ultrasound scan path delineation, path smoothing and checking, and robot-based ultrasound scan execution.

Keywords: ***surgical robotics, 3D ultrasound, navigation, path smoothing, normal determination, milling***

I. INTRODUCTION

Performing surgical procedures with the assistance of navigation or robotic systems usually consists of several pre-operative steps during the preparation phase (imaging and planning) and several intra-operative steps during the execution phase (registration and actual plan execution). Such computer- or robot-assisted surgery (*CAS/RAS*) systems only fully exhibit their benefits when operating on high resolution imaging data and good quality registration, i.e. successful determination of the geometric relationship between planning data and execution site. Traditionally, this is achieved with „gold standard" procedures, consisting of a computed tomography (*CT*) scan of the patient and inclusion of implanted or temporary artificial markers for registration in the operating room (*OR*). Precision requirements are especially high for surgical robots in orthopedic applications. With appropriate planning data, individual trajectories in optimally determined positions can be computed for the respective milling, drilling, or sawing operations. These need to be retrieved exactly by registration procedures in the OR to fully utilize the positioning precision of robots and the computer-assisted planning.

Addressing the most important drawbacks of this approach (time requirements, radiation exposure, and invasiveness) we present a robot-based 3D ultrasound scanning method to generate intra-operative global image data. The method produces data equivalent to that of traditional CT but is less costly and can be used to perform both intervention planning and registration. The patient is not exposed to x-ray radiation, and since the presented method is markerless – it does not rely on (implanted) pins – it can alleviate the need for time-consuming pre-operative preparation and imaging procedures. As registration between the patient and the corresponding image data is implicit in the presented scheme (imaging is performed just before the time of execution), planning and execution take place directly in the image data without any need for external registration methods (except between robot and image data).

The scope of application for the presented system is the automated milling of cavities in the lateral skull bone for subdermal implantation of hearing aids, where one process step is the removal of bone material from the thin skull bone

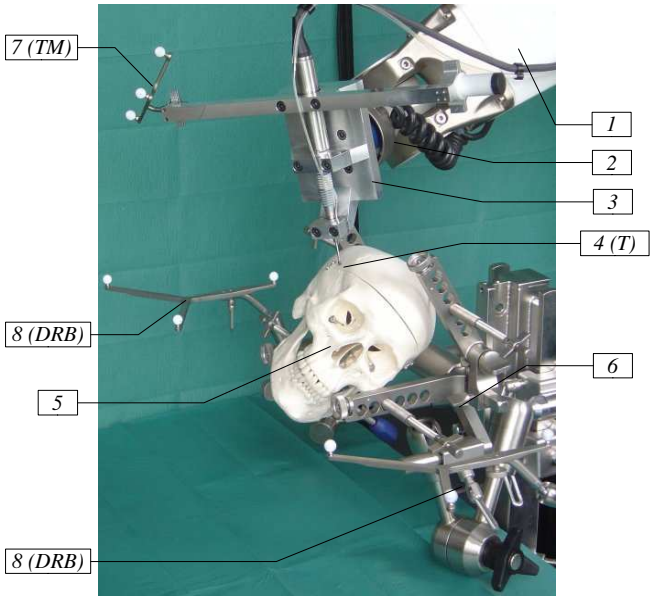

Figure 1: Setup of the RONAF system – robot arm (1) with force/torque (F/T) sensor (2), tool holder (3), surgical miller tip (4), skull phantom (5), fixtures (6), and infrared-reflective markers of the tool (7) and the robot base (8)

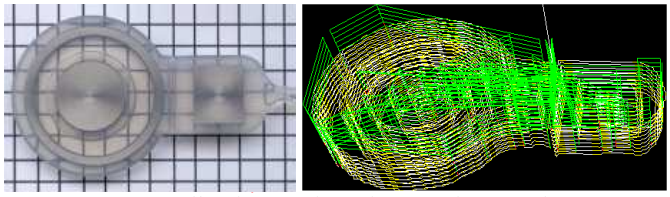

Figure 2: Soundbridge implant dummy (left; grid 5x5mm²), generated layered concentric milling path (right)

(*calotte*) in the shape of flat amplifier components (Figure 1, Figure 2) [6], [7]. Other applications would be *mastoidectomies* (removal of arbitrarily shaped bone volumes behind the ear) or generally any intervention where ultrasound data can effectively replace imaging, e.g. orthopedic knee or hip interventions.

Based on an overview of the state of the art (Section II), one can justify the development of a robot-based 3D ultrasound system and accompanying registration and checking procedures (Section III). The implementation for a specific application with a specific robot system (Section IV) is experimentally validated for the whole process on human preparations (Section V). Finally, the outlined conclusions indicate the possible direction of future work (Section VI).

II. State of the art

Currently, the standard imaging modality for planning in autonomous and/or cooperative robot-assisted surgery (*RAS*) systems is global preoperative data from CT, with magnetic resonance imaging (*MRT*) following closely. Examples are the commercial systems Robodoc [10] and CASPAR (orthopedic knee and hip interventions), the AcroBot (knee) [2], or research systems like RobaCKa [3] and CRANIO/CRIGOS (orthopedic interventions on the skull) [1]. They require lengthy imaging procedures before the intervention and some means of registering imaging data with the situation in the operating room.

Alternatives for certain limited cases include atlas- or model-based CT-free methods, e.g. by sampling bone surface regions of the knee or hip/knee pivot points with hand-held infrared navigation system pointers, thus fitting a generic organ model to patient-specific features (e.g. „BrainLab VectorVision knee“).

The use of ultrasound (*US*) has been traditionally limited for manual intervention planning purposes due to its low resolution. However, its non-invasive nature makes it the preferred choice for registration, as with tracked US A-mode (i.e. 1D) probes to register the patient with a prior CT scan, e.g. [17]. However, recent developments towards high-precision US systems enable their use at least for situations where the thickness of tissues with highly different densities needs to be measured [4], [12].

However, actual 3D ultrasound scanning for planning and registration can be found in only a small number of projects, e.g. in the IR-navigated B-mode (2D) manual scanning of the shoulder/elbow area with concurrent 3D volume reconstruction in [8]. As the resolution and precision of conventional US probes is low, this data is difficult to use for planning CAS/RAS interventions.

Finally, the combination of robot-based interventions with 3D ultrasound as the basis for planning (instead of CT) has not been presented in the literature, in spite of its potential advantages, such as non-invasiveness of imaging and registration, no radiation exposure, and potential high axial resolution.

III. Registration and Surface Scanning

Therefore, we can state our design requirements as follows: Discarding CT in favor of US imaging for orthopedic interventions makes high-precision measurements necessary, with distance and preferably bone thickness being sampled with a precision comparable to the ~0.4mm standard set by conventional CT. Furthermore, because the US probe is a local sensor (it does not provide global positioning information) we need a means of locating the samples relative to each other with a spatial and temporal precision resulting in volume reconstruction better than or comparable to CT. Finally, the volume needs to be *registered* to the robot precisely enough to be useful for navigation with additional local sensor support [18], i.e. the transformation from planning data to the robot coordinate system must be established.

With the presented method, several implicitly registered image modalities are generated for navigation. First, a skull surface representation is generated by manual sampling of surface points with a hand-held IR pointer, after which a skull representation is created by scanning the skull with a robot-held A-mode US probe, returning both outer and inner skull boundaries. Both representations can be used in addition to or as a replacement for a CT scan. Their acquisition automatically registers the robot with the patient.

To achieve this, several transformations – between the robot, optical tracking system, and IR pointers – need to be established first (Section A). Robot-based scanning relies on a manually defined path that has to be smoothed (Section B) before further processing (surface normals determination, Section C) takes place. Finally, path planning for the robot may bring about kinematic problems that need to be addressed before actual execution (Section D).

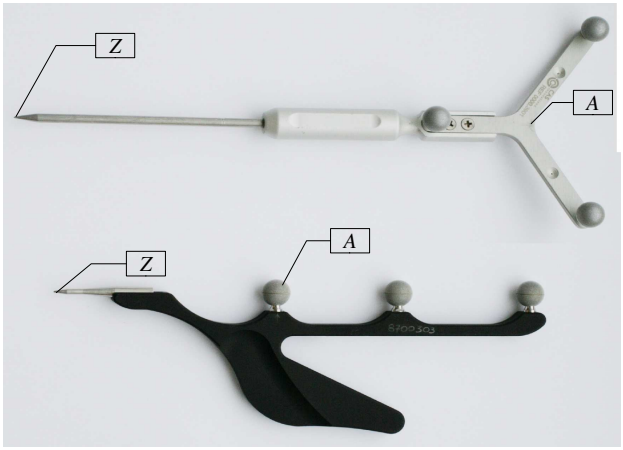

Figure 3: Two pointers (6D and 5D) with respective (example) local frames (origin A) and tips (Z)

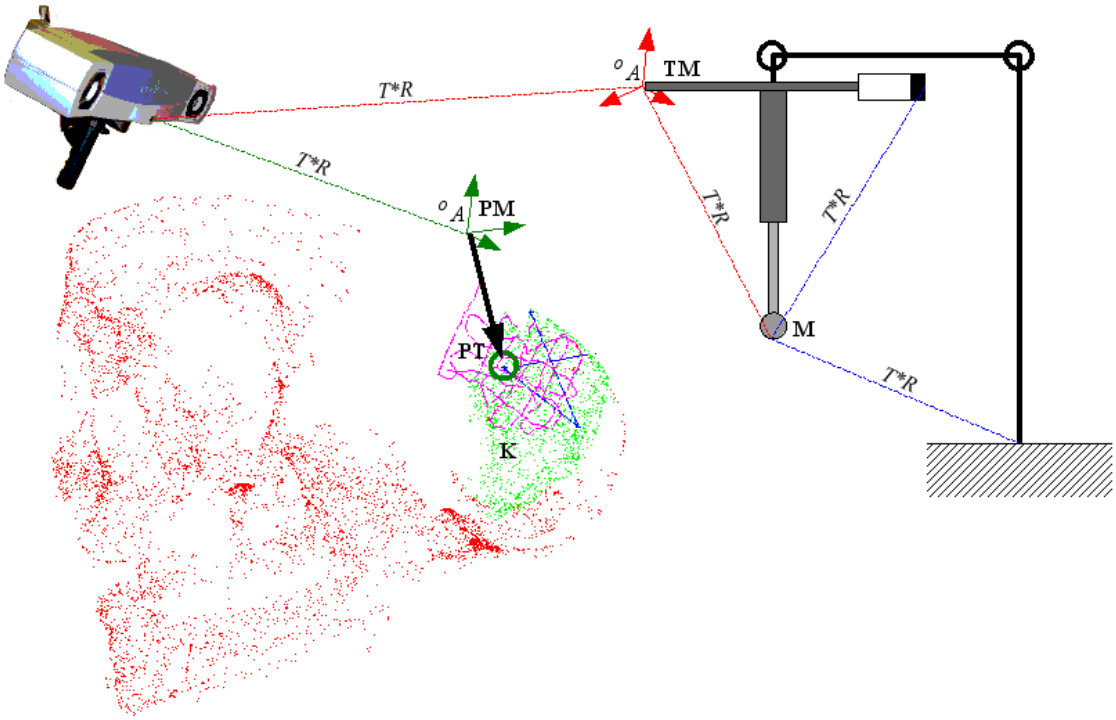

Figure 4: Registrations (3D – only translations T, 6D – translations T and rotations R) between robot and tool and US probe (tool tip M, tool infrared marker TM), the optical tracking system (OTS), skull surface and scan path (K) demonstrated by hand-held pointer (pointer tip PT, pointer infrared marker PM)

A. Registration of Robot, Optical Tracking, and Pointers

The registration relationships between the robot, optical tracking system (*OTS*), hand-held pointers, skull surface, and the US scan path for the presented system are shown in Figure 4. The rigid tool combination including miller and US probe forms one registration entity which needs to be registered to the actual patient in the operating room (*OR*). Since imaging data originates directly from the current patient situation (contrary to CT data which would need to be sampled separately beforehand), patient and bone representation can be identified as one entity which does not need any additional registration procedures. The milling volume (the implant bed) needs to be positioned within this representation, e.g. through a position optimization procedure as described in [14].

First, the robot performs calibration motions to calibrate the transformation between the milling tool and its rigidly attached IR marker and register both in OTS coordinates (Objects 4 and 7 in Figure 1). These motions consist of pivoting around the miller tip (to calibrate the exact position of the tip in its associated marker's coordinates, while it is known in robot coordinates) and subsequent translation motions along the tool X and Y axes (to determine the rotation between the OTS and tool marker coordinate systems). The pivoting motion results in a spherical cloud of marker positions samples by the OTS, which is then subjected to a sphe-

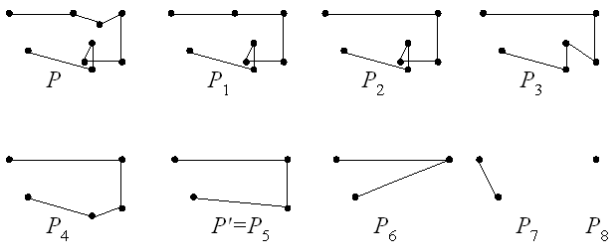

Figure 5: Example of complete smoothing of a two-dimensional path P with nine path points. In each step i, the path point whose removal leads to the smallest possible deviation between Pi and the original path P is removed. A reasonable smoothed path could be e.g. P_5

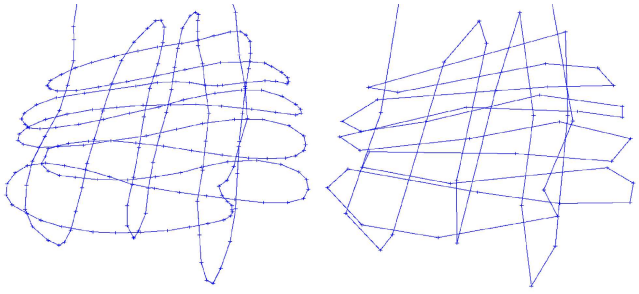

Figure 6: Scan path for ultrasound recording of the human skull – original path (left, 307 path points) and smoothed path using K_1 and d_s = 1.0mm (right, 90 path points)

re-fitting algorithm to compute the position of the sphere center, representing the miller tip [13], [9].

Second, the user calibrates a hand-held OTS pointer, determining the specific translation between pointer marker *A* and pointer tip *Z* (Figure 3), by pivoting it around its tip. The user then samples a cloud of skull surface points by sliding the pointer over the exposed skull, thus creating a surface representation which is already registered with the OTS, and thus with the robot.

Third, the pointer is used to define the 3D positions making up the scan path on the skull surface to be followed by the robot-held US probe. We allow the user to perform this step manually to allow explicit consideration or omission of problematic regions with strong curvature or sensitive structures. However, the US probe will need to be oriented almost perfectly perpendicular to the surface to be scanned in order to receive satisfying US echoes. This is especially important for correct delineation of the inner skull boundary. Therefore, the sequence of 3D points acquired needs to be processed prior to path execution by path smoothing and surface normal determination procedures.

B. Scan Path Smoothing

Let $P=\{p_1, ..., p_n\}$ be a path consisting of path points $p_i \in \Re^m$, m being the dimensionality of the path and n the number of path points. In order to allow faster and less jerky scanning, the scan path P is smoothed by successively removing points until the resulting path deviation exceeds an application-specific threshold [16]. In the following, the smoothing procedure we developed is explained.

We define the *neighborhood* of a path point p_i as the sequence of points in P between and including the two nearest neighbors of that point in the path P to the left and and right of p_i.

Let d_i be the *deviation* between the smoothed path P' and the original path P in the neighborhood of the path point p_i. The *error function* K represents the criterion used to compute d_i. Its input are the two paths P and P' as well as the index i, and its output is the deviation d_i between them. Finally, we need a threshold value d_s, indicating the maximum allowed d_i. The entire smoothing process uses the same K.

We implemented three error functions suitable for different applications. The deviations computed using these error functions extend over the neighborhood of a removed point.

- K_1: d_i is the maximum Euclidean deviation of the smoothed path from the original path in the neighborhood of p_i.
- K_2: d_i is the root-mean-square deviation of the path points in the original path from the shortened path.
- K_3: d_i is the area between the smoothed path and the original path.

Thus, we search for a path P' whose deviation from P does not exceed d_s at each individual path point according to K. The number of path points in path P' is minimized under the given conditions (Figure 5).

The algorithm for removing path points is described in detail in [16]. Figure 6 shows an initial US scan path and the result of path smoothing using error function K_1 and a maximum deviation of 1.0mm.

C. Surface Normals Determination

In the next step, surface normals over a local sample neighborhood are determined from the scan path and surface points.

Let $P = \{p_1, \ldots, p_n\}$ be a set of Cartesian 3D points with $p_i = (x_i, y_i, z_i)$. P can be conceived of as a point cloud approximating a possibly non-planar surface.
Furthermore, we need the center $m = (m_x, m_y, m_z)$, indicating the point for which the normal vector on the surface should be determined. It is not necessary that $m \in P$, and m needs not be contained in the surface defined by the point cloud, but ideally it should be close to it.

The algorithm can be subdivided into three steps. First, the space containing P is hashed allowing for fast access to neighboring points. This step must be performed only once per point cloud. The next two steps consist of finding the relevant points $n_i \in Q \subseteq P$ in the proximity of m and computing the normal vector on the surface defined by Q. These steps must be repeated for each normal vector.

The normal vector $N = (a, b, c)^T$ is directly related to the equation of the regression plane R that is the optimal approximation of the point cloud: $R = \min \{ a \cdot x + b \cdot y + c \cdot z + d \}$.

We have to find a, b, c and d so that

$$\min\left\{\sum_i (a\cdot x_i + b\cdot y_i + c\cdot z_i + d)^2\right\}, \quad i = 1,...n \Leftrightarrow$$

$$\min\left\{ n\cdot d^2 + \sum_i \begin{pmatrix} a^2\cdot x_i^2 + 2\cdot a\cdot x_i\cdot b\cdot y_i + 2\cdot a\cdot x_i\cdot c\cdot z_i \\ +2\cdot a\cdot x_i\cdot d + b^2\cdot y_i^2 + 2\cdot b\cdot y_i\cdot c\cdot z_i \\ +2\cdot b\cdot y_i\cdot d + c^2\cdot z_i^2 + 2\cdot c\cdot z_i\cdot d \end{pmatrix}\right\}, \quad i = 1,...n$$

$$=: \min\{f(a,b,c,d)\}$$

To avoid the trivial solution $(a, b, c, d) = (0, 0, 0, 0)$, we have to set one element $\neq 0$. Without loss of generality, let $a = 1$. Now, we can solve

$$f(a,b,c,d)|_{a=1} = \min\left\{ n\cdot d^2 + \sum_i \begin{pmatrix} x_i^2 + 2\cdot x_i\cdot b\cdot y_i + 2\cdot x_i\cdot c\cdot z_i + 2\cdot x_i\cdot d + \\ b^2\cdot y_i^2 + 2\cdot b\cdot y_i\cdot c\cdot z_i + 2\cdot b\cdot y_i\cdot d + c^2\cdot z_i^2 + 2\cdot c\cdot z_i\cdot d \end{pmatrix}\right\} \quad (1)$$

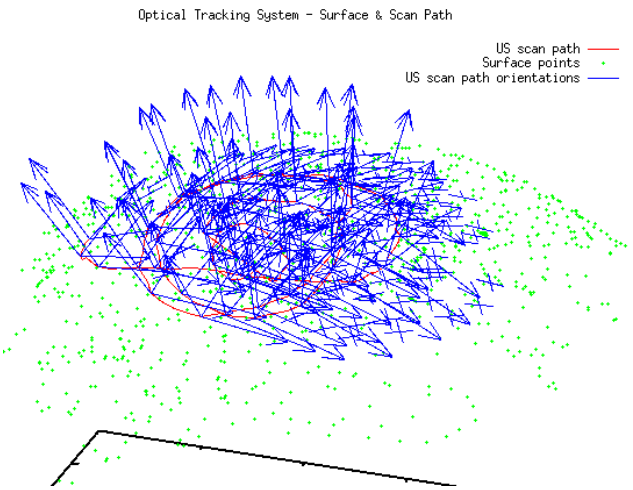

Figure 7: Surface points and US scan points (sampled with IR pointer) and computed orientations for roll v = -20°

In order to simplify the computations and avoid numerical errors, it is wise to shift P into its center of gravity. This way, the regression plane passes through the origin and $d = 0$.

Let $S_{a,b} =: \sum_{i=1}^{n} a_i \cdot b_i$ and $S_a =: \sum_{i=1}^{n} a_i$. By deriving Equation (1) by b and c respectively, we obtain the solutions

$$a = 1, b = \frac{S_{z,z} \cdot S_{x,y} - S_{y,z} \cdot S_{x,z}}{S_{y,z}^{\ 2} - S_{z,z} \cdot S_{y,y}} \text{ and } c = \frac{S_{x,z} \cdot S_{y,y} - S_{y,z} \cdot S_{x,y}}{S_{y,z}^{\ 2} - S_{z,z} \cdot S_{y,y}} \quad (2)$$

A multiplication by the common denominator yields the normal vector's components

$$N = \left(S_{y,z}^{\ 2} - S_{z,z} \cdot S_{y,y},\ S_{z,z} \cdot S_{x,y} - S_{y,z} \cdot S_{x,z},\ S_{x,z} \cdot S_{y,y} - S_{y,z} \cdot S_{x,y} \right).$$

If the plane is parallel (or close) to the (y, z) plane, the computation becomes unstable. Therefore, we repeat the computation with $b = 1$ resp. $c = 1$ instead of $a = 1$. The computation with the largest denominator in Equation (2) is the most precise one and is thus selected. Because at most one of the three computations can be numerically unstable (the regression plane can only be perpendicular to at most one main axis), the calculated result is valid.

Finding the normalized normal vector from n samples requires $6n$+11 additions, $6n$+21 multiplications and one division, i.e. the calculation has an asymptotic complexity O(n).

D. Robot-Based Ultrasound Scan Execution

The procedure described so far yields a 5D path – a sequence of 3D positions with two rotational degrees of freedom (*DOF*) fixed. This arrangement leaves each point with one DOF open; in the presented system this is the roll parameter, i.e. rotation around the long tool axis. Since the US probe operates in A-mode, each single shot is rotationally invariant around this DOF, which can therefore be set to any kinematically valid value between 0° and 360°.

By arbitrarily selecting one orientation around the US sensor axis, the scan path can be followed, guiding the probe perpendicularly to the skull surface (Figure 7). However, since robots usually have limited DOF and joint ranges, not every orientation results in a valid executable path. In the presented case, the robot has six non-redundant DOF, and following the the skull's curvature with the robot-held probe often leads to kinematic singularities and joint limit problems, compromising safety and leading to abortion of the current path execution. Therefore, the remaining DOF is used to alleviate those problems.

After registration of the robot, the patient, and the 5D path, a valid 6D path is searched from a set of paths generated with different roll values that are held constant over the whole path. First, a finite working set V of roll values is selected from a range that is (empirically) believed to contain values that will result in valid paths later. Second, all paths P_v corresponding to roll values $v \in V$ are generated and interpolated densely with respect to Euclidean distance and orientation. Finally, each P_v is validated by applying the robot inverse kinematics to each interpolated path point and checking for joint limits, singularities, and discontinuities (Figure 8). In the current implementation, the first completely traversable path is selected for execution. If no kinematically admissible path is found, the robot base location must be changed.

The final scan path execution with concurrent ultrasound sampling returns a sequence of US A-scans, with the single upper and lower skull boundaries detectable by thresholding the filtered radio-frequency signal. For better results, matched filtering is performed with coded excitation chirp signals. Instead of single ultrasound pings, a modulated waveform is emitted and cross-correlated with its echoes, thus improving detection in the face of bad signal-to-noise ratio [12].

This process creates two 2.5D skull boundary representations for implant position optimization [14]. As we now have two data sets describing the outer skull boundary – the US-based representation and the initial surface points sampled manually with the IR pointer – they can be combined to create an improved outer boundary description.

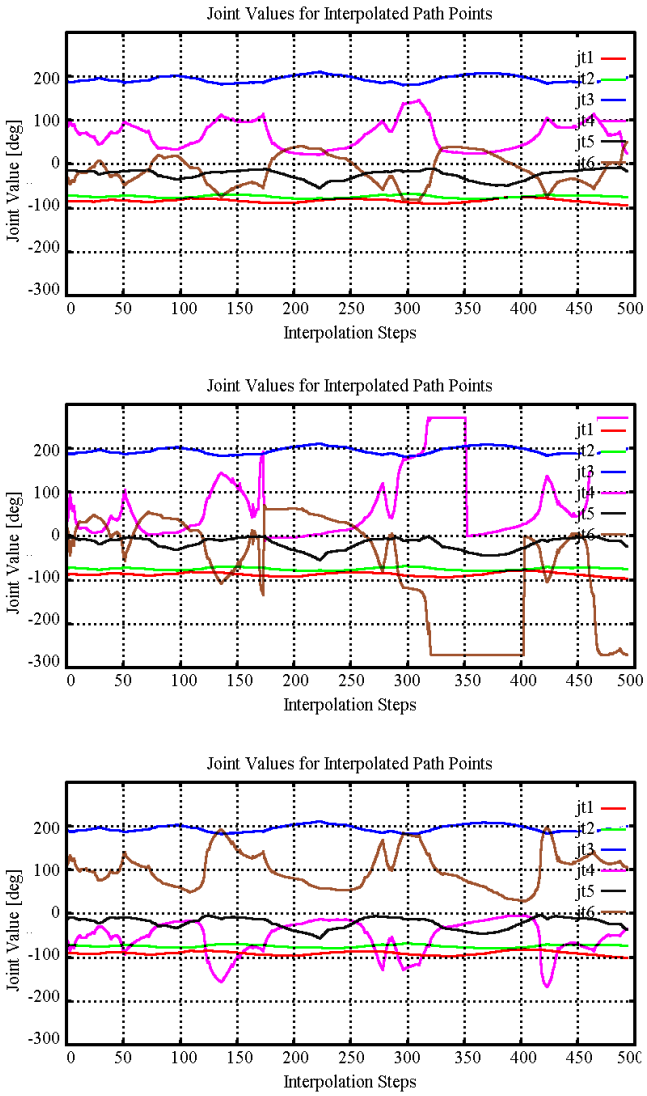

Figure 8: Joint value graphs for the presented robot's six joints; for roll v = -10° (top), 0° (centre), and +10° (bottom). The 0° path is invalid due to joint limit problems; note the close interaction between elbow and wrist joints 4 and 6 for all paths.

IV. Application and System

The validity of the presented method was tested on a system used for automated milling of cavities in skull bone for subdermal implantation of hearing aids. The RONAF project (*Robot-based Navigation for Milling at the Lateral Skull Base*, [6]) researches the feasibility and benefits of various navigation methods in autonomous surgical robotics. One step in the investigated process is the removal of bone material in the shape of flat amplifier components from the thin calotte (Figure 2).

The robot is an industrial model (Stäubli RX90) retrofitted with regard to speed and safety and used for medical use in hip and knee endoprosthesis milling applications (CASPAR, by Orto-Maquet). Sensors include – amongst others – a 6D force/torque (*F/T*) sensor (JR3 90M31A with strain gage bridges, max. sensing range 63N/5Nm, resolution 1:4000), an NDI Polaris infrared-optical tracking system (*OTS*; measured repeatability accuracy 0.05mm root-mean-square (*RMS*) after warm-up phase, specified absolute accuracy 0.35mm RMS, silo-shaped work volume ~(1000mm)³, data rate 20...60Hz), and a Transmit-Receive Module II ultrasound probe (*US*; by Fraunhofer IBMT, St. Ingbert/Germany). The US system control computer is connected with the robot for position acquisition via a local network. Using two ultrasound probes (center frequency 2,25 MHz, diameter ¼ in. and 1 MHz, diameter ½ in.) with flexible delay lines attached to the transducer, filtered and unfiltered radio frequency signals are available for signal processing. The tool is a surgical mill (electrically driven miller Aesculap microtron EC/GD622, up to 30.000 rpm) mounted perpendicularly to the robot tool flange to minimize deformation (Figure 1, cf. [9]).

V. Experiments and Results

We performed the entire described procedure on three human skull preparations (cf. Figure 9), including pointer and robot calibration and registration, sampling of skull surface points, demonstration and processing of scan paths, and their execution with concurrent US scanning.

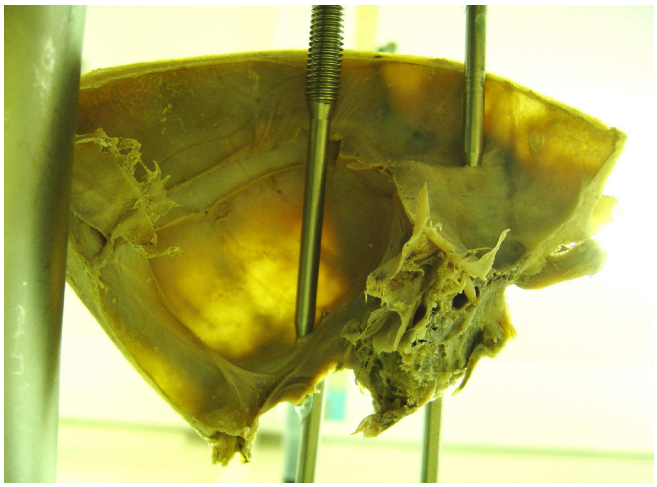

Figure 9: Image of human skull preparation. Bone thickness varies widely, affecting detection quality.

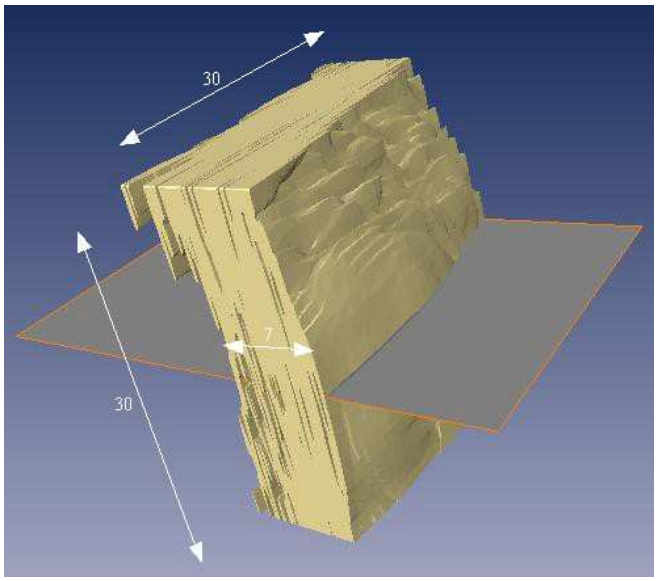

Figure 10: 3D ultrasound volume reconstruction (skull sample, probe guided by 3D µm positioner)

The manually generated surface point cloud is a 2.5D global map registered to the robot with a precision of <2.5mm RMS. This relatively large error stems from an accumulation of smaller error components. Looking closely at the procedure used to create this map, it is apparent that the calibration accuracy of the hand-held pointer, its position as reported by the OTS, the position of the tool marker as reported by the OTS, and the tool calibration accuracy all contributed to the sequential deterioration of the registration quality between the pointer and the tool tip (i.e. between map and robot). A more precise discussion of the definition and a measurement of this cumulative error can be found in [9]. The result of bad registration quality in this step is a map or a scan path whose representation in robot coordinates is not identical to its actual position, so following this path sometimes resulted in motions outside the actual volume of or within the skull bone. However, due to the flexible delay line attached to the front of the US probe, most scans could be completed successfully.

However, the US scan generates a map consisting of two 2.5D skull surface point clouds, both of which are registered to the robot with a precision equal to the robot's absolute positioning accuracy (close to the robot's relative accuracy of ~0.35mm) (Figure 10). Another factor in the scan map's precision is the accuracy of thickness detection in the single US shots, which is ~0.5mm (standard deviation for US pulse code excitation with direct coupling of transducer and bone [19]), but this value is highly patient-specific.

VI. Conclusions

We have described a process and an intuitive user interface for bone surface and ultrasound scan path input using an IR pointer registered with a robot, resulting in two global maps: a manually generated, navigation system-based surface map and a robot-based 3D ultrasound map with extracted skull boundaries. These maps are created and registered

non-invasively, thus representing an advance in RAS planning data acquisition.

With respect to the initial design requirements, we can state that the 3D ultrasound and surface maps created can be used for CT-free implant position optimization and milling path planning [15]. The US system itself can be used as an IR-tracked manual standalone system as well (SonoPointer®, [5]), allowing for creation of high precision 3D US scans with minimal hardware and software requirements. Bone thickness for single US samples can be measured with a precision of 0.5mm, comparable to CT. These measurements must be compiled into a reconstruction volume based on the spatial information supplied by robot encoders, resulting in a maximum expected ~0.85mm imprecision in the reconstruction, *including* registration error between reconstruction and robot. The precision of the 3D US volume reconstruction (robot-based or manual) compared to CT data must still be experimentally established, but is expected to be sufficient for navigation purposes, especially when supported by local navigation. The overall precision of the complete intervention, thus "closing the loop", will be investigated in future work.

Future work should also include force control of the contact between probe and skull during the scan. This would counteract bad tool-pointer registration quality and IR sensor noise as well as probe-surface contact errors arising from high surface curvature. Furthermore, scan path optimization with respect to variable probe orientations (or other open DOFs) will be necessary for reliable robot-assisted scanning, as there may be paths that are not traversable with constant values for the open DOFs, or which can be improved on a point-to-point basis with respect to joint velocities, collision avoidance or other criteria.

Acknowledgements

This work is a result of the project „Robot-based navigation for milling at the lateral skull base (RONAF)" of the special research cluster „Medical navigation and robotics" (SPP 1124) funded by the Deutsche Forschungsgemeinschaft (DFG), performed in cooperation with the Universitäts-HNO-Klinik (Abt. HNO-Heilkunde) in Heidelberg/Germany. Further information can be found at *http://ai3.inf.uni-bayreuth.de/projects/ronaf/.*

References

[1] G. Brandt, K. Radermacher, A. Zimolong, G. Rau, P. Merloz, T.V.S. Klos, J. Robb, H.W. Staudte, *"CRIGOS - Entwicklung eines Kompaktrobotersystems für die bildgeführte orthopädische Chirurgie"*, Orthopädie 2000 - 29:645-649, Springer-Verlag 2000.

[2] B.L. Davies, S.J. Harris, W.J. Lin, R.D. Hibberd, R. Middleton, J.C. Cobb, *"Active Compliance in robotic surgery – the use of force control as a dynamic constraint"*, Proc. Instn Mech Engrs, Part H, Journal of Engineering Medicine 211(4), 1997.

[3] D. Engel, J. Raczkowski, H. Wörn, *"RobaCKa: Ein Robotersystem für den Einsatz in der Chirurgie"*, Proc. Workshop 'Rechner- und sensorgestützte Chirurgie', eds. Wörn et al, Heidelberg 2001.

[4] P.A. Federspil, S.H. Tretbar, P.K. Plinkert, "*Increase the Accuracy in Navigated Surgery by in site Measurement of individual Sound Velocity in Skull Bone*", CURAC 2005, Berlin/Germany, September 2005.

[5] P.A. Federspil, S.H. Tretbar, C. Sittel, P.K. Plinkert, "*SonoPointer® - a prototype system for ultrasound scanning of skull bone thickness*", AORL 2006 (in Press).

[6] D. Henrich, "*Robotergestütztes Fräsen an der lateralen Schädelbasis: Kraft-basierte lokale Navigation bei der Implantatbettanlage*", Robotik 2002, Ludwigsburg/Germany, June 2002.

[7] D. Henrich, Ph. Stolka, "*Principles of Navigation in Surgical Robotics*", *MRVN 2004*, Remagen/Germany, March 2004.

[8] U. v. Jan, D. Sandkühler, L. Kirsch, H.-M. Overhoff, „*Definition of a humerus coordinate system from semiautomatically segmented 3-D ultrasound volumes*", Biomedizinische Technik (49) Ergänzungsband, Schiele&Schön, Berlin, 2004.

[9] Ph. Stolka, D. Henrich, „*Improving Navigation Precision of Milling Operations in Surgical Robotics*", IROS 2006, Beijing/China, 2006.

[10] R.H. Taylor et al, „*An image-directed robotic system for precise orthopaedic surgery*", IEEE Transactions on Robotics and Automation 10(3):261-275, June 1994.

[12] S. H. Tretbar, Ph.A. Federspil, P.K. Plinkert, "*Improved ultrasound based navigation for robotic drilling at the lateral skull base*", CARS 2004

[13] D. Umbach, K.N. Jones, "*A Few Methods for Fitting Circles to Data*", IEEE Transactions on Instrumentation and Measurement, 2000.

[14] M. Waringo, Ph. Stolka, D. Henrich, *"First System for Interactive Position Planning of Implant Components"*, *CURAC 2003*, Nürnberg/Germany, 2003.

[15] M. Waringo, D. Henrich, „*3-Dimensionale schichtweise Bahnplanung für Any-Time-Fräsanwendungen*", VDI Robotik 2004.

[16] M. Waringo, D. Henrich, „*Efficient Smoothing of Piecewise Linear Paths with Minimal Deviation*", IROS 2006, Beijing/China, 2006.

[17] S. Winter, B. Brendel, A. Rick, M. Stockheim, K. Schmieder, H. Ermert, „*Registrierung 3-dimensionaler CT- und Ultraschalldaten anhand von Knochenstrukturen*", 1. Jahrestagung der Deutschen Gesellschaft für Computer- und Roboter-assistierte Radiologie und Chirurgie (CURAC), Leipzig/Germany, 2002.

[18] Ph. Stolka, D. Henrich, „*Building Local Maps in Surgical Robotics*", IROS 2005, Edmonton, Alberta/Canada, 2005.

[19] S.H. Tretbar, Ph.A. Federspil, C. Günther, P.K. Plinkert, *„Ultraschall-Dickenmessung der Schädelkalotte zur Registrierung bei navigierten Eingriffen an der lateralen Schädelbasis"*, Biomedizinische Technik 2004, 49 Ergänzungsband 2 (858-859), 2004.